# Computational study of blood flow in lower extremities under intense physical load

**Article** *in* Russian Journal of Numerical Analysis and Mathematical Modelling · October 2013

DOI: 10.1515/rnam-2013-0027

CITATIONS
31

READS
172

**3 authors:**

Sergey S Simakov
Moscow Institute of Physics and Technology
**96** PUBLICATIONS **483** CITATIONS
SEE PROFILE

T.M. Gamilov
I.M. Sechenov First Moscow State Medical University
**29** PUBLICATIONS **161** CITATIONS
SEE PROFILE

Yan Soe
Moscow Institute of Physics and Technology
**3** PUBLICATIONS **35** CITATIONS
SEE PROFILE

pp. 1–16 (2013)

# Computational study of blood flow in lower extremities under intense physical load

S. SIMAKOV*†, T. GAMILOV*, and Y. N. SOE*

**Abstract** — This work is aimed at computational study of the blood flow in lower extremities under intense physical load. We present a modified 1D cardiovascular system model describing skeletal-muscle pumping and autoregulation effects on the blood flow in lower extremities. Skeletal-muscle pump effect is introduced as an external time-periodical pressure function applied to a group of veins. The period of this function is associated with the two-stride period during running. The computational study reveals the explicit optimal stride frequency providing the maximum blood flow through the lower extremities. It is shown that the optimal stride frequency depends on personal parameters. The model is validated by a comparison to the stride frequencies of a number of top-level athletes, therefore, providing a method to assess the level of physical conditioning.

The state-of-the-art modern cardiovascular system simulations include 1D flow modelling in the network of elastic tubes [3, 6, 8, 15, 16], which is in some cases extended by 3D models for local regions resulting in the fluid-structure interaction problem [6] and multidimensional 1D–3D coupling [5, 6]. Most works in this field consider a normal or quiet state of the organism. A deeper look into the cardiovascular system simulation should include the physiological reactions of the vessel walls [3, 9] and their interaction with surrounding tissues, which is especially important for physical activity simulations.

This work is focused on the mathematical model of the cardiovascular system capable to simulate the blood flow under a physical load. We use a 1D network dynamical model of global circulation [8, 16] taking only systemic circulation. This model is supplemented with the models of vascular autoregulation and skeletal-muscle pump, including venous valves. Along with general pressure and velocity profile adjustments, we validate this model by the comparison of its response to the laboratory observations for the cases of gravitational and occlusion sampling tests and a changing body's orientation in the gravitational field.

We have limited our discussion by periodic activity associated with lower extremities muscles. That can also be associated with short-distance running. The mean blood flow in the anterior tibial vein is mainly observed as a measure of the lower extremities muscle blood supply. The considered simulations reveal the de-

*Moscow Institute of Physics and Technology, Dolgoprudny 141700, Russia

†Corresponding author. E-mail: simakov@crec.mipt.ru

This work was partially supported by the grants RFBR 11-01-00855-a, 11-01-00971 and MK 2719.2012.9.

pendence of the average blood flow and the stride frequency during walking and running. As a result, we observe the particular value of the stride frequency providing the maximum average blood flow in the anterior tibial vein that is associated with the optimal stride frequency. This value is calculated and compared for several top-level athletes. Good coincidence allows us to conclude that it could be a measure of a sportsman's efficiency.

## 1. Methods

### 1.1. Systemic circulation

As a core model for blood circulation we have used 1D network dynamical model [8, 16] taking into account the systemic arteries and veins. The model is based on the model of a viscous incompressible fluid flow through a network of elastic tubes. The flow in every vessel is described in terms of the mass and momentum balance:

$$\frac{\partial S_k}{\partial t} + \frac{\partial \left(S_k u_k\right)}{\partial x} = 0 \tag{1.1}$$

$$\frac{\partial u_k}{\partial t} + \frac{\partial \left(u_k^2/2 + p_k/\rho\right)}{\partial x} = f_{\mathrm{fr}}\left(S_k, u_k, S_k^0\right) + g\sin\theta_k \tag{1.2}$$

where $k$ is an index of the vessel, $t$ is time, $x$ is the distance along the vessel counted from the vessel junction point, $\rho$ is the blood density (a constant), $S_k(t,x)$ is the vessel cross-section area, $p_k$ is blood pressure, $S_k^0$ is the unstressed cross-sectional area, $u_k(t,x)$ is the linear velocity averaged over the cross-section, $g$ is the gravity constant, $\theta_k$ is the angle between the vessel and the gravity field, $f_{\mathrm{fr}}$ is the friction force given by

$$f_{\mathrm{fr}}\left(S_k, u_k, S_k^0\right) = -\frac{4\pi\mu u_k}{S_k^2}\left(\frac{S_k}{S_k^0} + \frac{S_k^0}{S_k}\right) \tag{1.3}$$

and $\mu$ is the blood viscosity.

In the statement of the boundary conditions it must be taken into account that equations (1.1) and (1.2) are hyperbolic. Boundary conditions for this type of equations shall be set allowing for the behaviour of the characteristic curves on the boundary of the integration domain. Namely, at any moment of time within the period considered, the number of the boundary conditions at each point of the boundary must correspond to the number of characteristic curves going out of the domain at this point. Simultaneously, the conditions imposed by the equations of the characteristic curves entering the domain (compatibility conditions) must be included. Therefore, it is essential to determine the behaviour of the characteristic curves of equations (1.1) and (1.2). Denoting

$$\mathbf{V}_k = \{S_k, u_k\}, \quad \mathbf{F}_k = \{S_k u_k, u_k^2/2 + p_k/\rho\}, \quad \mathbf{g}_k = \{\varphi_k, \psi_k\}$$

we write equations (1.1) and (1.2) in a divergence form:

$$\frac{\partial \mathbf{V}_k}{\partial t} + \frac{\partial \mathbf{F}_k}{\partial x} = \mathbf{g}_k.$$

Then, using the scalar multiplication by the left eigenvectors $\boldsymbol{\omega}_{ki}\,(i=1,2)$ of the Jacobi matrix $\mathbf{A}_k = \partial\mathbf{F}_k/\partial\mathbf{V}_k$ we obtain the characteristic form of (1.1) and (1.2)

$$\boldsymbol{\omega}_{ki}\cdot\left(\frac{\partial\mathbf{V}_k}{\partial t}+\frac{\partial\mathbf{F}_k}{\partial x}\right)=\boldsymbol{\omega}_{ki}\cdot\left(\frac{\partial\mathbf{V}_k}{\partial t}+\lambda_{ki}\frac{\partial\mathbf{V}_k}{\partial x}\right)=\boldsymbol{\omega}_{ki}\cdot\mathbf{g}_k,\quad i=1,2 \tag{1.4}$$

where $\lambda_{ki}$ are the eigenvalues of the matrix $\mathbf{A}_k$.

The specific expression for $\mathbf{A}_k$, by definition

$$\mathbf{A}_k=\frac{\partial\mathbf{F}_k}{\partial\mathbf{V}_k}=\begin{pmatrix} u_k & S_k \\ \dfrac{1}{\rho}\dfrac{\partial p_k}{\partial S_k} & u_k \end{pmatrix}.$$

Eigenvalues $\lambda_{ki}$ can be found from

$$\det(\mathbf{A}_k-\lambda_k\mathbf{E})=0,\quad \mathbf{E}=\begin{pmatrix}1&0\\0&1\end{pmatrix}$$

the solution of this equation is given by

$$\lambda_{ki}=u_k+(-1)^i\sqrt{\frac{S_k}{\rho}\frac{\partial p_k}{\partial S_k}},\quad i=1,2. \tag{1.5}$$

The left eigenvectors $\boldsymbol{\omega}_{ki}$ are determined from the equations (except for the constant factor)

$$\boldsymbol{\omega}_{ki}(\mathbf{A}_k-\lambda_{ki}\mathbf{E})=0,\quad i=1,2$$

and it is possible to choose, for example

$$\boldsymbol{\omega}_{ki}=\left\{\sqrt{\frac{1}{\rho}\frac{\partial p_k}{\partial S_k}},(-1)^i\right\},\quad i=1,2. \tag{1.6}$$

The value $\sqrt{(S_k/\rho)\,(\partial p_k/\partial S_k)}$ from (1.5) is the velocity of small disturbances. In all parts of the cardiovascular system during the normal functioning and in the cases of most pathologies, the velocity of small disturbances is bigger than the blood flow velocity $u_k$. For such flows, as follows from (1.5), at each point of the considered domain at any moment of time one of the characteristic curves has a positive slope and the other one has a negative slope. In the statement of the boundary conditions, therefore, only one condition should be set at the inlet and the outlet of the elastic tube.

At the entry point of the vessel connected to the heart, the blood flow is assigned as the boundary condition

$$u(t,0)\,S(t,0)=Q_H\,(t)\,. \tag{1.7}$$

At the terminal point of the venous system ($x = x_H$) the pressure is set as the boundary condition

$$p_H(t, x_H) = p_H. \tag{1.8}$$

At the vessels junctions the Poiseuille's pressure drop condition and the mass conservation condition are posed

$$p_k\left(S_k\left(t,\tilde{x}_k\right)\right) - p^l_{\text{node}}\left(t\right) = \varepsilon_k R^l_k S_k\left(t,\tilde{x}_k\right) u_k\left(t,\tilde{x}_k\right), \quad k = k_1, k_2, \ldots, k_M \tag{1.9}$$

$$\sum_{k=k_1,k_2,\ldots,k_M} \varepsilon_k Q_k\left(t,\tilde{x}_k\right) u_k\left(t,\tilde{x}_k\right) = 0 \tag{1.10}$$

where $M$ is number of the connected vessels, $\{k_1, \ldots, k_M\}$ is the range of the indices of the connected vessels, $p_{\text{node}}(t)$ is the pressure at the junction point, $\varepsilon = 1$, $\tilde{x}_k = 0$ for the incoming vessels, $\varepsilon = -1$, $\tilde{x}_k = L_k$ for the outgoing vessels.

Every boundary condition (1.7)–(1.10) is supplemented with the compatibility condition of the hyperbolic set (1.1), (1.2). After finite differences discretization it provides a linear dependence between the linear velocity $u_k(t_{n+1}, \tilde{x}_k)$ and the cross-section area $S_k(t_{n+1}, \tilde{x}_k)$ at the upper time layer at the end or at the beginning of every vessel composing a node

$$u_k(t_{n+1}, \tilde{x}_k) = \alpha_k S_k(t_{n+1}, \tilde{x}_k) + \beta_k. \tag{1.11}$$

The nonlinear set (1.9)–(1.11) of $2M+1$ equations can be reduced to the set of $M$ equations [4] and can be effectively solved by the Newton method.

The coefficients $\alpha$ and $\beta$ for (1.11) can be derived using finite differences discretization of (1.4) (index $k$ is suppressed, but implicitly assumed until the end of this section). For each vessel we use a uniform 1D mesh

$$M = \left\{ (x_j, t_n) : x_j = hj,\ hJ = L,\ j = 0, \ldots, J;\ t_n = \sum_{p=1}^{n} \tau_p \right\}$$

where $h$ is the spatial step, $\tau_p$ is the $p$-th time step. For the beginning of the vessel outgoing from the node we are looking for $\mathbf{V}(0, t_{n+1})$ taking $\mathbf{V}(0, t_n)$ from the previous time step and $\mathbf{V}(x_1, t_{n+1})$ from the internal points explicit computational algorithm [4]. Taking

$$\left(\frac{\partial \mathbf{V}}{\partial x}\right)_{0,t_{n+1}} \approx \frac{\mathbf{V}(x_1, t_{n+1}) - \mathbf{V}(0, t_{n+1})}{h}, \quad \left(\frac{\partial \mathbf{V}}{\partial t}\right)_{0,t_{n+1}} \approx \frac{\mathbf{V}(0, t_{n+1}) - \mathbf{V}(0, t_n)}{\tau_{n+1}}$$

$$(\boldsymbol{\omega}_i)_{0,t_{n+1}} \approx (\boldsymbol{\omega}_i)_{0,t_n}, \quad (\lambda_i)_{0,t_{n+1}} \approx (\lambda_i)_{0,t_n}$$

and denoting

$$w = \sqrt{\frac{1}{\rho}\left(\frac{\partial p}{\partial S}\right)}_{0,t_n}, \quad \mathbf{W} = \{w, (-1)^i\}, \quad \sigma = \frac{\tau_{n+1}}{h}\left(\lambda_i\right)_{0,t_n}$$

we can discretize (1.4) for the inlet ($i = 1$) as

$$\mathbf{W} \cdot \left( \frac{\mathbf{V}(0,t_{n+1}) - \mathbf{V}(0,t_n)}{\tau_{n+1}} + (\lambda_i)_{0,t_n} \frac{\mathbf{V}(x_1,t_{n+1}) - \mathbf{V}(0,t_{n+1})}{h} \right) = \mathbf{W} \cdot \mathbf{g}. \quad (1.12)$$

That can be rewritten in form (1.11) taking

$$\alpha = w$$
$$\beta = \frac{w(\sigma S(x_1,t_{n+1}) - S(0,t_n)) + u(0,t_n) - \sigma u(x_1,t_{n+1}) - \tau_{n+1}(w\varphi - \psi)}{1-\sigma}.$$

The same method applied to the outlet conditions results in

$$\alpha = -w$$
$$\beta = \frac{w(\sigma S(x_{J-1},t_{n+1}) + S(x_J,t_n)) + u(x_J,t_n) + \sigma u(x_{J-1},t_{n+1}) + \tau(w\varphi + \psi)}{1+\sigma}.$$

### 1.2. Wall-state equation

The elastic properties of the vessel wall material are described by the wall-state equation providing response to the transmural pressure (the difference between the blood pressure and the pressure in the tissues surrounding the vessel):

$$p_k(S_k) - p_{*k} = \rho c_k^2 f(S_k) \quad (1.13)$$

where the $S$-like function $f(S)$ is approximated as

$$f(S_k) = \begin{cases} \exp\left(S_k/S_k^0 - 1\right) - 1, & S_k > S_k^0 \\ \ln\left(S_k/S_k^0\right), & S_k \leqslant S_k^0 \end{cases} \quad (1.14)$$

and $p_{*k}$ is the pressure in the tissues surrounding the vessel, $c_k$ is the small disturbance propagation velocity of the wall material in the relaxed state ($S_k = S_k^0$), which can be interpreted as the pulse wave velocity (PWV) in the unstressed vessel [19].

As is shown in Section 2, the purely mechanical model presented in this section fails to describe correctly some of the features related to the transient states, e.g. the changing body orientation in the gravity field, vessel occlusion, and others. Real vascular networks include the regulatory and venous blood return mechanisms (muscle pump, venous valves, respiratory pump etc. [14]) that can substantially affect the pressure and velocity profiles. Some of these effects are introduced in the following section.

### 1.3. Autoregulation

We consider blood flow autoregulation as the response of the arteries wall elasticity to changes in the averaged blood parameters (such as mean pressure, mean blood

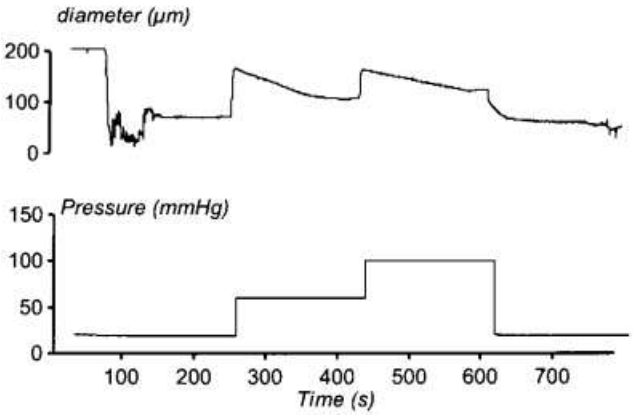


**Figure 1.** The effect of subsequent pressure steps on diameter of rat artery [1].

flow, or oxygen concentration). A laboratory study presented in Figure 1 reveals the vessel's initial expanding (passive phase) and subsequent gradual contraction (active phase) under the induced blood pressure increase. It results in maintaining a constant mean blood flow despite the changes in pressure.

Autoregulation is a local effect occurring even in isolated blood vessels. According to [7], there are many potentially important mechanisms of autoregulation: myogenic, metabolic, tissue pressure, etc. Each mechanism has its own experimental evidence. We are using only the myogenic hypothesis in this work, as it has a straightforward mechanical interpretation and probably plays the dominant role under intensive physical loads considered in this work.

According to the myogenic hypothesis, the vascular smooth muscle responds to variations in the mean pressure. A mean pressure increase produces contraction in the vascular smooth muscle, which results in the vessel's increased stiffness, consequently providing a higher pulse wave velocity. The same is valid for a mean pressure decrease resulting in the vascular smooth muscle relaxation and decreasing both stiffness and pulse wave velocity.

The vascular smooth muscle cells responding to the mean pressure variations are located in tunica media (the middle layer of a blood vessel wall). This layer is quite thick in arteries and relatively thin in veins. As a result, myogenic autoregulation in veins provides no substantial impact on the blood flow and we remove it from consideration.

These observations may be incorporated in our model as follows. The cross-section area $S_k$ and blood pressure $p_k$ are related by the parameter $c_k$. Assuming the cross-section area to be constant and applying (1.13) to it, we will derive the following dimensionless time-independent parameter

$$\frac{\overline{p}_k - \overline{p}_{*k}}{\rho c_k^2} = \overline{f(S_k)} = \text{const}. \tag{1.15}$$

It requires a computational algorithm modification. Autoregulation is not an instant

process. To avoid significant changes in the vessel properties during a single heart period, we should take an average of (1.15) over the time. Assuming $\overline{p}_{*k} = 0$ in the arteries and $\rho = \text{const}$ we have

$$\frac{\overline{p}_k}{c_k^2} = \text{const}. \tag{1.16}$$

Taking the average pressure during two subsequent averaging periods $T_1$, $T_2$ throughout the vessel $k$ we can recalculate the new value $c_k$ for the next period $T_3$ and so on:

$$\frac{c_{k,\text{new}}}{c_{k,\text{old}}} = \sqrt{\frac{\overline{p}_{k2}}{\overline{p}_{k1}}} \tag{1.17}$$

where $\overline{p}_{kj}$ is the average transmural pressure for the averaging period $T_j$. The shortest averaging period should be greater or equal to the heart period, as the mean pressure may substantially change during shorter periods. We use 4 seconds for all averaging periods, as it provides a more stable solution in our numerical experiments. This value is substantially smaller than a characteristic time of the simulations, that is 100–200 seconds.

### 1.4. Skeletal-muscle pump

In this work we consider physical load specific for running. It is characterized by periodic activity of the muscles of the lower extremities. Due to the anatomical structure the skeletal-muscle pump does not affect large arteries [14] and we remove them from further consideration. Assuming the force compressing the vein to be directed perpendicularly to its axis enables us to relate muscle pumping to external pressure $p_{*k}$ in (1.13). The maximum value of this pressure may be derived if we consider muscle as a cylinder holding the weight of a human body, which gives us [11]:

$$p_{*k} = \frac{mg}{S}\frac{\sigma}{1-\sigma} \tag{1.18}$$

where $m$ is the mass of the body, $S$ is the muscle average cross-section, $\sigma$ is the muscle's Poisson ratio. Taking for a trained athlete $m = 60\,\text{kg}$, $\sigma = 0.49$ and $S = 600\,\text{cm}^2$ we evaluate $p_{*k}$ as 10 kPa.

We consider running as a periodical process with a period $T$. This period is equal to the time needed for two complete strides. Thus the stride frequency is

$$\nu = \frac{2}{T}. \tag{1.19}$$

As a result, muscle-pumping pressure can be given by

$$p_{*k} = \frac{P_{\max}}{2}\left(1 + \sin\left(\frac{2\pi t}{T} + \Phi\right)\right) \tag{1.20}$$

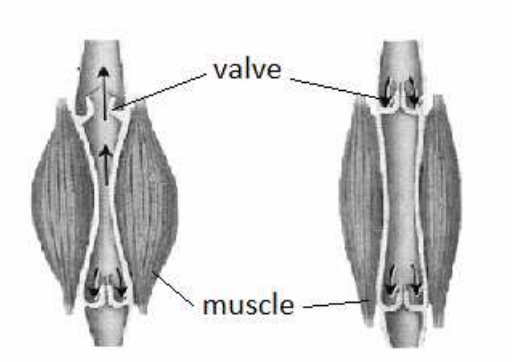


**Figure 2.** Venous valves.

where $P_{\max} = 10\,\text{kPa}$, $\Phi$ is the phase ($\Phi_l = 0$ for the left leg and $\Phi_r = \pi/2$ for the right leg).

The additional feature of the major leg veins significant for muscle-pumping is the valve functioning preventing the backward blood flow [14]. The mechanism of the valve functioning is shown in Fig. 2.

We propose to simulate this feature by modifying friction force (1.3) as

$$F_{\text{fr}} = \begin{cases} f_{\text{fr}}(s,u), & u > 0 \\ A, & u < 0 \end{cases} \tag{1.21}$$

where $f_{\text{fr}}(s,u)$ is friction force used in a general non-valved vessel (1.3), $A \gg f_{\text{fr}}$ (in this study $A = 100\,f_{\text{fr}}$) is a virtual force used to prevent the backward flow. It differs of course from the actual venous valve functioning. Here we implicitly assume the instant venous valve activation immediately after the linear velocity comes below zero. For the real case a small time-lag is observed and some relatively small negative value of the linear velocity may be achieved. We neglect this kinetic energy losses, especially within the scope of the short-time simulations performed in this work.

### 1.5. Integration domain and model identification

We suppose that the networks of arteries and veins have the same structure. The corresponding vessels have the same length $\left(L_k^{\text{art}} = L_k^{\text{ven}}\right)$, the diameters of the corresponding veins are twice as large as those of the arteries $\left(d_k^{\text{art}} = 2d_k^{\text{ven}}\right)$. The total network of systemic circulation is composed by joining the arterial and venous networks by virtual vessels having averaged properties corresponding to the peripheral circulation. The parameters of these terminal vessels were specified to contain about 20% of the total blood volume and provide the adequate pressure and blood velocity difference between the arteries and veins according to [14]. The general scheme of the network is shown in Fig. 3. The structural and functional parameters of the network were specified according to the available data [14, 15, 17]. A more detailed

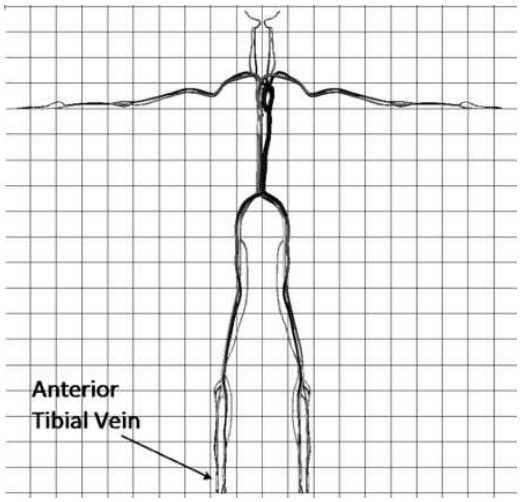


**Figure 3.** The scheme of arterial and venous vessel networks.

description of the methods of integration and model identification can be found in [8, 16].

The specific case considered in this work relates to cardiovascular simulation under an intense physical load. This is generally applicable to sportsmen and other specially trained persons. We use the PWV index to specify the vessel wall elasticity more adequately, since trained athletes are characterized by increased elasticity and, consequently, lower PWV values [12, 13]. The vascular network was also fitted to the body height by appropriate scaling of the vessel lengths.

## 2. Results

The developed model has been identified, tested and validated by different methods described in [8, 16]. Most related works just provide pressure, linear velocity or blood flow profile adjustment to some laboratory or generally known physiology data. This of course confirms the models. For the case of physical activity simulations where autoregulation plays an important role it is also important to adjust the model response to some static and dynamical disturbances. In the beginning of this section we validate our model by comparing its response to laboratory observations for the cases of gravitational and occlusion sampling tests and the changing body orientation in the gravitational field. The rest of the section presents the results of the computational study of the blood flow in lower extremities under an intense physical load.

### 2.1. Model validation

The scheme of gravitational sampling is presented in Fig. 4. The arterial volume distensibility was experimentally measured in [20] from the electrocardiogram and

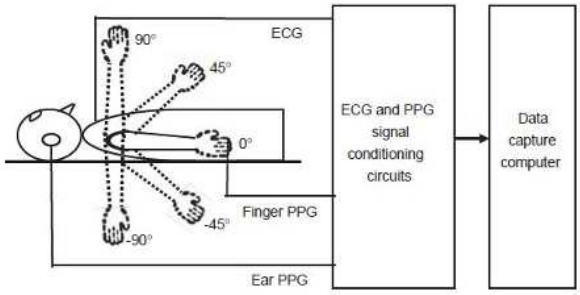


**Figure 4.** The scheme of the experiment [20].

the finger and ear photoplethysmogram records from 15 subjects with the right arm at five different positions (90°, 45°, 0°, −45° and −90° degrees with respect to the horizontal level). By definition, the arterial volume distensibility $D_v$ gives a relative blood volume change in a selected vascular region with a known change in arterial pressure

$$D_v = \frac{1}{\Delta P}\frac{\Delta V}{V}.$$

According to [20] it can be rewritten as

$$D_v = \frac{1}{\rho a^2} \tag{2.1}$$

where $a$ is the pulse wave velocity. Formula (2.1) is used for the validation of the model presented in this work.

The experimental series described in [20] were simulated by our model. The results of numerical simulations are presented in Fig. 5 along with the data from [20]. The conclusion is that they are in quite good qualitative and even quantitative agreement.

The occlusion sampling test is described in [10]. It involves measuring the Peripheral Arterial Tone (PAT) signal from a finger during brachial artery occlusion. Healthy subjects show an increased PAT signal during recovery, which corresponds to the average blood pressure increase in the peripheral arteries, while unhealthy subjects with inadequate autoregulation show a blunted response. The results of numerical simulation of this test are shown in Fig. 6. We only mention the qualitative coincidence here, since the available analog PAT signal is not directly recalculated to pressure. In most cases a higher average pressure leads to a higher arterial tone and PAT amplitude, but it can be invalid for some specific cases, such as obstructive sleep apnea [18].

The next dynamic test of our model is based on the simulation of the body orientation in the gravitational field. It is known that a change in the body position from horizontal to vertical one causes the blood pressure increase, e.g. in the anterior tibial artery. The cross-section initially increases and then returns towards its normal level due to the autoregulation effect. In this simulation we have considered the

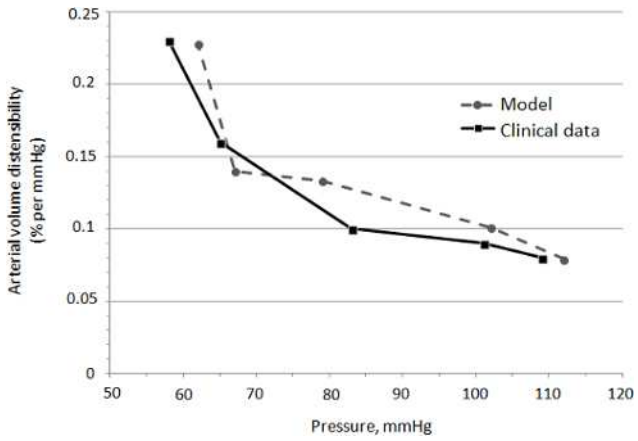


**Figure 5.** Relationship between mean arterial pressure and arterial volume distensibility.

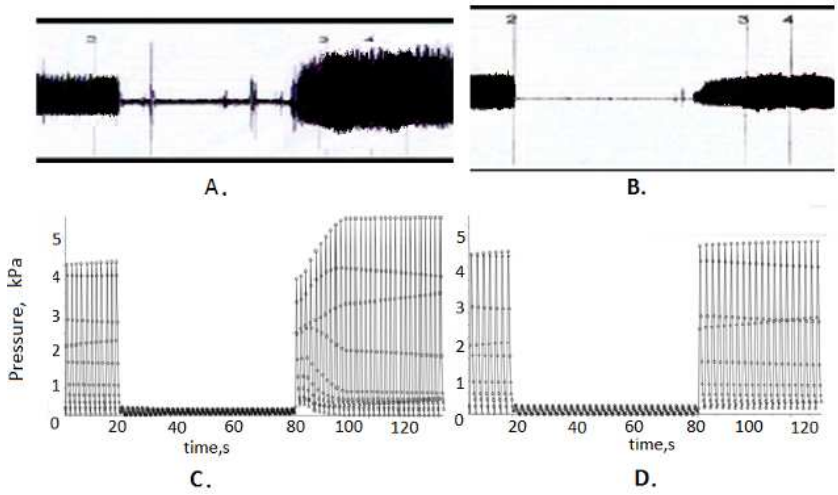


**Figure 6.** A and B are PAT signals (measured from a finger) during cuff occlusion [10] for healthy and diseased subjects. C and D are numerically calculated pressure in a finger during occlusion with and without autoregulation.

vascular network to be at rest for the first 80 seconds. After that a gravitational impact is activated by the right part of (1.2). We assume it corresponds to the body position changing from horizontal to vertical. The calculated anterior tibial artery cross-sections with the time are shown in Fig. 7. Qualitatively the model behaviour corresponds to the loaded rat arteries behavior [1] presented in Fig. 1.

Figure 7 shows that the model with autoregulation is capable of providing a correct response to some external disturbances, such as the body position change. After standing up, the leg arteries contract to neutralize the blood pressure increase in the lower extremities. An excessive blood pressure in the lower body could lead to an

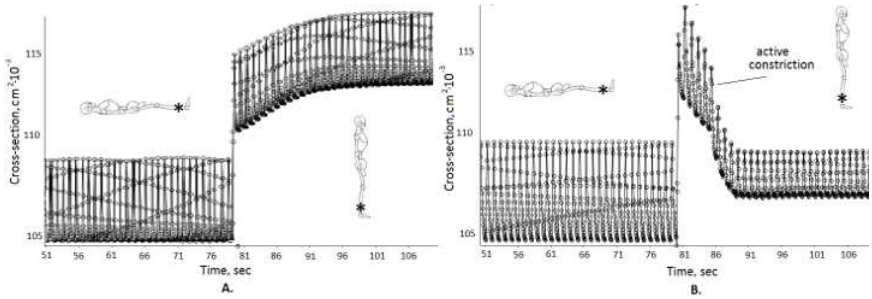


**Figure 7.** The effect of changing body position on cross-section of anterior tibial artery without (A) and with (B) autoregulation.

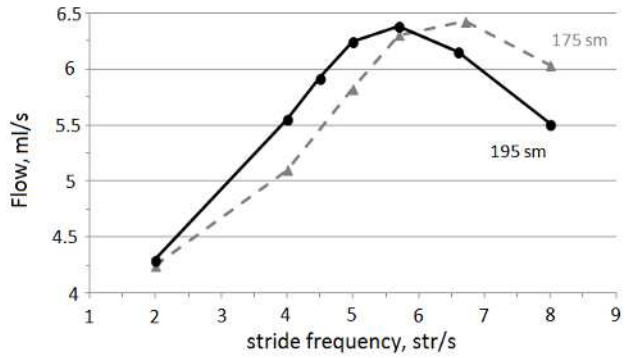


**Figure 8.** Stride frequency for the networks fitted to the body height of 175 cm and 195 cm.

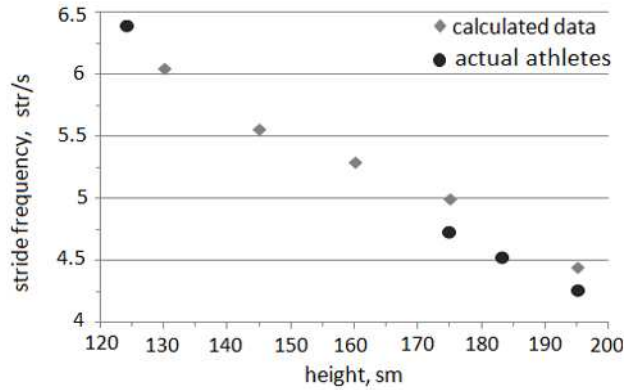


**Figure 9.** Optimal stride frequency for trained athletes.

increased load on the venous valves resulting in their malfunctioning. This, in turn, is the reason for such vascular decease as varicose veins etc. The other important physiological reason for maintaining blood pressure in the lower body at the same level as before standing is to neutralize the sudden pressure drop in the brain. The sudden pressure drop in the upper body could be the reason for orthostatic hypotension [2], such as dizziness, blurred or dimmed vision, or even faint. It is especially important for adults generally experiencing regulatory mechanism malfunctions.

### 2.2. Skeletal-muscle pump

The developed model allows us to simulate the blood flow in legs during an intense exercise, taking into account the specific vessel elasticity of trained athletes and their height. In each simulation we consider the vascular network to be at rest for the first 90 seconds to assure the pseudo steady pulsate state maintained all over the network. After that an external pressure (1.20) is applied to the leg veins for the following 70 seconds. Mainly the anterior tibial vein (see Fig. 3) was observed. The blood flow was averaged over 4 cardiac cycles. The results of the first series include the simulations of the mean blood flow in the tibial vein for different stride frequencies (see Fig. 8). From Figure 8 one can observe an increase in the blood flow, along with the stride frequency increase until some optimal value is achieved. A further increase in the stride frequency results in the blood flow decrease. We regard this value as the optimal stride frequency, since it provides the maximum blood supply, consequently, resulting in the maximum muscles oxygen supply due to convective transport by blood.

The next computational series showed that the optimal stride frequency depends on the total length of the vessel network and the elastic properties of the vessel walls and does not depend on the boundary conditions for the heart. In the simulations presented in this work the elastic properties were set according to the PWV data for trained athletes [12, 13]. Figure 8 demonstrates the stride frequency dependence on the body height. In this simulations the vessel lengths were fitted to the height by linear scaling

$$L_{k2} = \frac{H_2}{H_1} L_{k1} \tag{2.2}$$

where $H_{1,2}$ is the height of the body in two simulations, $L_{k1,2}$ is the length of the $k$-th vessel in two simulations.

More detailed computational analysis is presented in Fig. 9. The optimal stride frequency is simulated for several selected body heights. It is compared to several well-known results in the recent world-level competitions. We selected the gold (A) and bronze (B) medal winners in 100 meters sprint in Beijing 2008 Olympiad, the bronze medal winner in 100 meters sprint in London 2012 Olympiad (C) and the gold medal winner in 100 meters sprint in World Dwarf Games 2008 (D). The actual sportsmen's stride frequency and height was measured from the free online video available in the World Wide Web. These parameters are summarized in Table 1.

From Fig. 9 one can observe quite good agreement between the simulated and

**Table 1.**
Actual parameters of the athletes. A, B, C, and D notations are presented in the text.

| | A | B | C | D |
|---|---|---|---|---|
| Height, cm | 195 | 175 | 183 | 124 |
| Stride frequency, str/sec | $4.27 \pm 0.05$ | $4.7 \pm 0.1$ | $4.54 \pm 0.02$ | $6.40 \pm 0.05$ |

the actual optimal stride frequencies within a wide range of heights. We should mention that the model used for these simulations provides rather a qualitative than a quantitative description. It includes some physiological effects, such as muscular pumping with venous valves and the myogenic autoregulation mechanism. But many other important effects, such as metabolic and tissue pressure autoregulation mechanisms, other regulatory systems, the heart rate variability, oxygen transport, respiratory system, energy production and release by the organism, and others are not included. Nevertheless, the computed values are very close to the actual data (see Fig. 9). It provides evidence of the valid blood flow simulation under an intense physical load using the proposed approach. Further simulations are needed to validate this model, which should include more of different athletes specializing in long-distance running as well.

## Conclusion

It should be pointed out that the above numerical experiments in computing the optimal stride frequency consider the blood flow optimization for sprinters. But the period of 70 seconds selected for calculating the optimal stride frequency is far beyond the actual time needed to finish 100 meters distance, which is less than 10 seconds. The model application is also limited by the fact that a 4 second period is selected for averaging the mean blood pressure for the next stage controlled by the autoregulation response of again 4 seconds. It should also be mentioned that blood supply plays a minor role for short-distance runners, since the major energy is anaerobically produced by tissues. So if sprint is considered, there is no direct analogy with a real competition, even if actual parameters are set for simulations. In addition, the computational domain structure used in this work is quite far from the real vascular network, as only the major arteries and veins are included and only systemic circulation is considered.

Inlet and outlet boundary conditions (1.7)–(1.8) on the vascular network corresponding to the heart junctions cannot guarantee the mass conservation in the system in general. Nevertheless, a wide range of previously performed simulations revealed good quantitative coincidence in the quiet state of the system [4, 8, 16]. In the case of the intense physical load such approach produces more error. Along with the other assumptions, such as a constant heart rate and the absence of the baroreflex regulation, it will be one of the central questions of future studies. We have just used this simplified approach for a very limited time range (less than 70 seconds). Thus the model sensibility to these effects is negligible. We also conclude that the

flow maximum at the optimal stride frequency is mostly related to the local elastic properties of the lower extremities region.

We can assume that professional sprinters have stride frequencies that are very close to the optimal ones. It might be due to a natural inbred talent or years of hard work. It is possible to adjust the vessel elastic properties via combining endurance- and strength-based exercises. It looks like the elite sprinters train their circulatory system (involuntarily) in a way that their optimal frequency and the stride frequency are very close.

Nevertheless, it seems that the optimal stride frequency computed by our method strongly correlates with the observations. It seems to be a possible measure of a sportsman's efficiency, as far as ordinary organism simulations provide greater deviations from this value. Such simulations cannot be presented in systematic way due to substantial variability in untrained persons. Moreover, it may provide a more realistic criterion if other sport events with periodical physical loads and longer time periods would be considered. This is a starting point for the evolution of the present study.

## References

1. E. VanBavel, J. P. Wesselman, and J. A. Spaan, Myogenic activation and calcium sensitivity of cannulated rat mesenteric small arteries. *Circ. Res.* (1998) **82**, 210–220.
2. J. G. Bradley and K. A. Davis, Orthostatic hypotension. *Amer. Fam. Physician* (2003) **68**, No. 12, 2393–2399.
3. A. Ya. Bunicheva, M.A. Menyailova, S. I. Mukhin, N. V. Sosnin, and A. P. Favorskii, Investigation of influence of gravitational overloads on parameters of blood flow in the systemic circulation. *Matem. Model.* (2012) **24**, 67–82 (in Russian).
4. Yu. Vassilevski, S. Simakov, V. Salamatova, Yu. Ivanov, and T. Dobroserdova, Numerical issues of modelling blood flow in networks of vessels with pathologies. *Russ. J. Numer. Anal. Math. Modelling* (2012) **26**, No. 6, 605–622.
5. T. K. Dobroserdova and M. A. Olshanskii, A finite element solver and energy stable coupling for 3D and 1D fluid models. *Comp. Meth. Appl. Mech. Engrg.* (2013) **259**, 166–176.
6. L. Formaggia, A. Quarteroni, and A. Veneziani, *Cardiovascular Mathematics*. DE: Springer, Heidelberg, 2009.
7. P. C. Johnson, Autoregulation of blood flow. *Circ. Res.* (1986) **59**, 482–495.
8. A. S. Kholodov, Some dynamical models of external breathing and blood circulation regarding to their interaction and substances transfer. In: *Comp. Model. Med. Progr.*, Science, Moscow, 2001, 127–163.
9. N. Kudryashov and I. Chernyavskii, Numerical simulation of the process of autoregulation of the arterial blood flow. *Fluid Dynamics* (2008) **43**, No. 1, 32–48.
10. J. T. Kuvin, A. R. Patel, K. A. Sliney, N. G. Pandian, J. Sheffy, R. P. Schnall, R. H. Karas, and J. E. Udelson, Assessment of peripheral vascular endothelial function with finger arterial pulse wave amplitude. *Amer. Heart J.* (2003) **146**, 168–174.
11. L. D. Landay and E. M. Lifshitz, *Theory of Elasticity*. Elsevier, Oxford, 1986.
12. T. Otsuki, S. Maeda, M. Iemitsu, Y. Saito, Y. Tanimura, R. Ajisaka, and T. Miyauchi, Rela-

tionship between arterial stiffness and athletic training programs in young adult men. *Amer. J. Hypertens* (2003) **146**, 168–174.

13. R. Sala, C. Rossel, P. Encinas, and P. Lahiguera, The continuum of pulse wave velocity from young elite athletes to uncontrolled older patients with resistant hypertension. *J. Hypertens* (2010) **28**, 19.216.
14. R. F. Schmidt and G. Thews, *Human Physiology*. Springer-Verlag, Berlin–Heidelberg–New York, 1983.
15. S. J. Sherwin, L. Formaggia, J. Peiro, and V. Franke, Computational modelling of 1D blood flow with variable mechanical properties and its application to the simulation of wave propagation in the human arterial system, *Int. J. Numer. Meth. Fluids* (2003) **43**, No. 6–7, 673–700.
16. S. S. Simakov and A. S. Kholodov, Computational study of oxygen concentration in human blood under low frequency disturbances. *Math. Model. Comp. Simul.* (2009) **1**, No. 2, 283–295.
17. S. Standring, *Gray's Anatomy: The Anatomical Basis of Clinical Practice*. Elsevier, Churchill-Livingstone, 2008.
18. D. P. White, Monitoring peripheral arterial tone (PAT) to diagnose sleep apnea in the home. *J. Clin. Sleep. Med.* (2008) **4**, No. 1, Suppl. 3, 73.
19. I. B. Wilkinson, J. R. Cockcroft, and D. J. Webb, Pulse wave analysis and arterial stiffness, *J. Cardiovasc. Pharmacol.* (1998) **32**, Suppl. 3, S33–7.
20. D.Zheng and A. Murray, Non-invasive quantification of peripheral arterial volume distensibility and its non-linear relationship with arterial pressure *J. Biomech.* (2009) **42**, 1032–1037.